Poziotinib Inhibits HER2-Mutant–Driven Therapeutic Resistance and Multiorgan Metastasis in Breast Cancer

Rashi Kalra[1,2], Ching Hui Chen[1,2], Junkai Wang[1,3], Ahmad Bin Salam[4], Lacey E. Dobrolecki[1], Alaina Lewis[1], Christina Sallas[1], Clayton C. Yates[4], Carolina Gutierrez[1], Balasubramanyam Karanam[4], Meenakshi Anurag[1,2], Bora Lim[1,2], Matthew J. Ellis[1,2], and Shyam M. Kavuri[1,2]

ABSTRACT

The pan-HER tyrosine kinase inhibitor (TKI) neratinib is therapeutically active against metastatic breast cancers harboring activating HER2 mutations, but responses are variable and often not durable. Here we demonstrate that recurrent HER2 mutations have differential effects on endocrine therapy responsiveness, metastasis, and pan-HER TKI therapeutic sensitivity. The prevalence and prognostic significance may also depend on whether the HER2 mutant has arisen in the context of lobular versus ductal histology. The most highly recurrent HER2 mutant, L755S, was particularly resistant to neratinib but sensitive to the pan-HER TKI poziotinib, alone or in combination with fulvestrant. Poziotinib reduced tumor growth, diminished multiorgan metastasis, and inhibited mTOR activation more effectively than neratinib. Similar therapeutic effects of poziotinib were observed in both an engineered HER2L755S MCF7 model and a patient-derived xenograft harboring a HER2G778_P780dup mutation. Overall, these findings support the need for clinical evaluation of poziotinib for the treatment of HER2-mutant metastatic breast cancer.

Significance: Evaluation of the functional impact of HER2 mutations on therapy-induced resistance and metastasis identifies robust antitumor activity of poziotinib and supports the clinical evaluation of poziotinib in ER^+ HER2 mutant breast cancer.

Introduction

Targeting amplification of the ErbB2 receptor tyrosine kinase gene (*ERBB2*), also known as human epidermal growth factor receptor 2 (HER2), is one of the greatest successes in oncology. A wide array of anti-HER2 agents have been developed, including monoclonal antibodies and conjugates [trastuzumab (Herceptin), trastuzumab emtansine (T-DM1), as well as small-molecule inhibitors (lapatinib, neratinib, and afatinib; ref. 1]. A decade ago, The Cancer Genome Atlas revealed an alternative HER2 activation mechanism in the form of somatic mutations, which occur across multiple cancer types (2–4). Subsequently, we and others demonstrated that HER2 somatic mutations are therapeutic targets in estrogen receptor positive (ER^+) non–HER2-amplified breast cancer and other cancers (5–16). The frequency of HER2 mutations in primary ER^+ breast cancer is approximately 3%. However, the prevalence is higher in metastatic breast cancers that have progressed upon endocrine therapy or CDK4/6 inhibitors (up to 6%), because they may drive acquired resistance to these standard-of-care agents (12, 17). HER2 mutations are also enriched in lobular carcinoma, where the rate is approximately 5%–26% (14, 18, 19). Despite the evident molecular and clinical heterogeneity, there has been only limited work on allele-specific HER2 mutation effects. Therefore, we hypothesized that individual mutations are associated with distinct therapeutic responses, metastatic propensity, patient outcome, and their association with lobular versus ductal ER^+ breast carcinoma. The importance of testing these issues is highlighted by the variable clinical activity of the irreversible pan-HER tyrosine kinase inhibitor (TKI) neratinib in phase II clinical trials (NCT01670877 and NCT01953926) across multiple different cancer types (9, 11, 20). Accumulated data show only a modest initial response to neratinib in ER^+ metastatic breast cancers, and response durations are typically short (9, 11, 20). Currently, neratinib as a single agent is not approved for HER2-mutant breast cancer because of limited clinical activity. In the present study, we sought to elucidate the impact of recurrent HER2-mutant alleles on endocrine therapy and neratinib response, multiorgan metastasis, and patient outcomes, parsed by lobular versus ductal histology. Additionally, we examined an alternative small-molecule inhibitor, poziotinib, to overcome therapeutic resistance and metastasis in HER2-mutant ER^+ breast cancer. These findings provide a rationale to investigate the clinical efficacy of poziotinib in HER2-mutant-driven metastatic breast cancer patients.

Materials and Methods

Clinical data sets

Genomic sequencing data and clinical outcome data associated with tumor samples from patients with primary or metastatic breast cancer in METABRIC 2012 and 2016 ($N = 2{,}509$), and MSK/IMPACT 2018 ($N = 1{,}918$) were accessed online via cBioPortal. From these data sets, ER^+ invasive lobular carcinoma (ILC) and invasive ductal carcinoma (IDC) were selected to examine the prevalence of HER2 missense mutations or insertions and HER2 amplification. For survival analysis, we used the overall survival (OS) or disease-free survival data of ER^+

[1]Lester and Sue Smith Breast Center, Baylor College of Medicine, Houston, Texas. [2]Department of Medicine, Baylor College of Medicine, Houston, Texas. [3]Department of Molecular and Cellular Biology, Baylor College of Medicine, Houston, Texas. [4]Department of Biology and Center for Cancer Research, Tuskegee University, Tuskegee, Alabama.

Corresponding Authors: Shyam M. Kavuri, Lester and Sue Smith Breast Center, Department of Medicine, Baylor College of Medicine, One Baylor Plaza, Houston, TX 77030. Phone: 1314-651-3876; E-mail: meghashyam.kavuri@bcm.edu; and Matthew J. Ellis, Lester and Sue Smith Breast Center, Baylor College of Medicine, One Baylor Plaza, Houston, TX 77030. E-mail: matthew.ellis@bcm.edu

Cancer Res 2022;82:2928–39

doi: 10.1158/0008-5472.CAN-21-3106

and HER2 nonamplified patients from the METABRIC cohort. HER2 amplification status was determined by copy number available in cBioPortal. Clinical information on HER2 somatic mutation and HER2 amplification status in ER^+ ILC and IDC breast cancer patients in both METABRIC and MSK-IMPACT studies is listed in Supplementary Table S1.

Cell lines

The ER^+ lobular breast cancer cell line MDA-MB-134 (MM134) was purchased from the ATCC. MM134 cells were cultured in DMEM: Leibovitz-15 1:1 media supplemented with 10% FBS and 1% penicillin/streptomycin. MCF7 breast cancer cell line (HER2 WT or the L755S HER2-activating mutation) were previously isogenically modified using AAV-mediated gene targeting as previously described (16). These MCF7 breast cancer cells were gifts from Dr. Ben Ho Park (Vanderbilt University Medical Center, Nashville, TN). These cells were cultured in IMEM supplemented with 10% FBS and 1% penicillin/streptomycin. SUM44PE cells were purchased from BIOIVT. SUM44PE parental or CRISPR knock in (KI) V777L and L755S cells were cultured in Ham's F12 media with 2% FBS and 1% penicillin/streptomycin supplemented with all the additional components listed in Supplementary Table S2 as per BIOIVT recommendations. For low E2 growth conditions, the appropriate phenol-red-free medium supplemented with 5% charcoal-dextran-stripped serum was used. All cell lines were cultured in 5% CO_2 at 37°C and were examined every 6 months for *Mycoplasma*.

Antibodies and inhibitors

Antibodies used for immunoblotting were purchased from Cell Signaling Technologies: phospho-HER2 (1248), phospho-p44/42 MAPK (Thr202/Tyr204), p44/42 MAPK, phospho-Akt (Ser473), Akt, phospho-S6 (240-44), phospho-S6 (235-236), phospho-MTOR, phospho-S6 (Thr 389), E-Cadherin (24E10); from Millipore: phospho-HER2 (pY1248); from Sigma: monoclonal Anti-β-Actin; and from Thermo Fisher: HER2 antibody (Ab-17). Poziotinib and tucatinib were obtained from Selleckchem. Pyrotinib was obtained from MedChem Express. Neratinib was provided by Puma Biotechnology, Inc., under a Materials Transfer Agreement.

Retroviral transduction of HER2 mutants in lobular breast cancer cell line

HER2 WT, S310F, L755S, and L869R retroviral vectors were transfected in the ØNX amphotropic packaging cell line. The HER2 WT, S310F, L755S, and L869R recombinant retroviral supernatants were used to transduce the MM134 cell line as shown previously (21). After 2 to 3 weeks of zeocin selection of bulk infected cultured cells, transgene expression was verified by fluorescence-activated cell sorting analysis for GFP expression (always >90%). Immunoblot analysis was performed on polyclonal cell lines to confirm HER2 protein expression.

CellTiter-Glo viability assays

For cell viability assay, cells were plated in opaque 96-well plates (costar, 3917) at 10,000 MM134 cells/well or 3,000 MCF7 cells/well and treated with drugs at the indicated concentrations for 30 days. After drug treatment (drug-containing media were changed twice a week), the cell culture medium in 96-well plates was replaced with 100 μL fresh medium per well and brought to room temperature. CellTiter-Glo (Promega, G7572) was added to each well (100 μL), and cells were lysed for 2 minutes at ∼250 rpm and then equilibrated at room temperature for 20 minutes. A plate reader was programmed to integrate luminescence for 500 ms per well. Viable cell luminescence was measured and plotted as relative luminescence units.

Immunoblot analysis

Cells were washed with cold PBS and lysed on ice in RIPA lysis buffer (Thermo Scientific; Pierce, 89900) containing protease and phosphatase inhibitors (Roche). Protein concentration in cell lysates was measured using BCA protein assay reagent (Bio-Rad). Cell lysates (25–30 μg) were subjected to SDS-PAGE followed by wet-transfer to nitrocellulose membranes (Invitrogen). The Invitrogen NuPage gel system was used. Nitrocellulose membranes were cut horizontally to probe with multiple antibodies. All primary antibodies were diluted in 5% BSA and incubated with blots overnight at 4°C. Blots were washed with 1 × TBST (3 times 8 minutes each) and incubated with horseradish peroxidase-conjugated secondary antibodies for 1–2 hours at room temperature followed by detection of immunoreactive bands by enhanced chemiluminescence (ECL, GE Healthcare, RPN2235).

Fat pad xenografts

MM134 parental, MM134-HER2 WT, MM134-HER2 S310F, and MM134-HER2 L755S were cultured in DMEM: Leibovitz 15 1:1 media supplemented with 10% FBS. MCF7 L755S KI cells were cultured in IMEM supplemented with 10% FBS and 1% penicillin/streptomycin. Cells were harvested and resuspended in media supplemented with 2% FBS and injected along with an equal volume of Matrigel into right side #4 mammary fat pads of 4-week-old NOD-*scid* gamma mice (Jackson Laboratory; NOD.Cg-Prkdcscid Il2rgtm1Wjl/SzJ Stock No: 005557). Tumor size was evaluated twice weekly by caliper measurements, and the volume of the mass was calculated using the formula $4/3 \times \pi \times (d/2)^2 \times (D/2)$, where d is the minor tumor axis and D is the major tumor axis. All values for tumor growth curves were recorded blindly. Established tumors (average volume, 250–400 mm^3) were randomized to the indicated treatment groups. For mouse xenograft experiments, 17 β-estradiol (cat. #E2758; Sigma) was maintained in 200-proof ethanol as a 2.7 mg/mL stock solution and added to drinking water twice a week at a final concentration of 8 μg/mL. Fulvestrant concentrations of 250 mg/kg body weight were prepared in corn oil freshly on day of injection (once a week) and administered subcutaneously. Neratinib 40 mg/kg and poziotinib 10 mg/kg were given in the form of chow, prepared by Research Diets Inc. Animals were sacrificed when tumors reached 1,500 mm^3 or at the study end time point. Tumors and organs were harvested and frozen in liquid nitrogen for storage or fixed in 10% neutral buffered formalin overnight at room temperature and then held in 70% ethanol. All animal procedures were approved by the Institutional Animal Care and Use Committee at Baylor College of Medicine (protocol #AN-7662).

Mouse intraductal model

MM134 parental, MM134-HER2 WT, MM134-HER2 S310F, and MM134-HER2 L755S were cultured in DMEM: Leibovitz 1:1 medium supplemented with 10% FBS. Cells were harvested and resuspended in 2% FBS in PBS at a concentration of 20,000 cells/μL. 80,000 cells were intraductally injected into the right #4 mammary gland of 8–10-week-old NOD-scid gamma (NSG) mice. Upon injection, mice were randomized to receive either filtered water or filtered water supplemented with 17 β-estradiol as indicated earlier. Injected mice were imaged using IVIS and palpated for tumors weekly. 100 μL of 15 mg/mL D-luciferin was used per mouse for IVIS imaging. Bioluminescence was quantified with the LivingImage software (Perkin Elmers). Tumor size was evaluated weekly by caliper measurements, and the volume of the mass was calculated as above. Mice were euthanized when tumors

reached 1,500 mm^3. *Ex vivo* imaging was also performed, and tissues were fixed in 10% neutral buffered formalin overnight at room temperature and then held in 70% ethanol. All animal procedures were approved by the Institutional Animal Care and Use Committee as above.

RNA sequencing

MM134 cells stably transfected with HER2 WT or HER2 L755S were deprived of E2 by incubation in charcoal-stripped FBS-containing media for 7 days. RNA was isolated from two replicates each of cells using the GE Healthcare Illustra RNA spin mini kit (cat. #25-0500-71) according to the manufacturer's instructions. The Genomic and RNA Profiling Core (GARP) at BCM constructed libraries with 250 ng of total RNA using the TruSeq RNA Library Prep Kit (Illumina). cDNA was generated from poly(A)-selected RNA. Libraries were quantified with the KAPA Library Quantification Kit (Kapa Biosystems) and were sequenced on the NovaSeq 6000 (Illumina). Alignments were performed against human genome version GRCh38 using the STAR program. Differential expression analysis was determined through edgeR. Gene set enrichment analysis (GSEA) was done with the preranked tool on the ranked gene list. Genes were ranked based on signed *P* value, which was calculated as the sign of log2-fold change * −log10 (adj *P* value). RNA sequencing data of estrogen-deprived MM134 WT and L755S cells shown in this study have been submitted to Gene Expression Omnibus Accession Number GSE197952.

IHC

IHC staining was executed with the help of the Pathology Core at the Lester and Sue Smith Breast Center, Baylor College of Medicine. Tissue sections were incubated at 58°C overnight in a dry slide incubator and deparaffinized in xylene and graded alcohol washes. Antigen retrieval was performed in 0.1 M Tris-HCl pH 9.0 (*p*-HER2 and ERα), followed by quenching in 3% H_2O_2. The following antibodies were used to stain for 1 hour at room temperature: ERα (clone 6F11, Novocastra, 1:200) and p-HER2 (Cell Signaling, 2243L, 1:50). After washing in TBS, EnVision labeled polymer-HRP anti-mouse or anti-rabbit antibodies (Dako) were added for 30 minutes at room temperature. Slides were washed with TBS and then developed with DAB^+ solution (Dako) and DAB sparkle enhancer (Biocare). After washing in TBS, slides were counterstained with hematoxylin, dehydrated, and cleared before coverslipping with Cytoseal (VWR). p-HER2 and ER^+ stained cells were quantified in lung/ovary sections of L755S fat pad (FP) xenografts and ovary sections from HER2 WT and HER2 S310F or L755S MIND xenograft mice.

Schrödinger methods: glide ligand docking

The ligands neratinib and poziotinib were docked into HER2 kinase domain L755 (PDB ID: 3PP0) by utilizing the Glide module of Schrödinger suite Maestro V12.3. The mutant HER2 L755S was created in Schrödinger suite Maestro V12.3. The docking was performed utilizing Standard precision (XP) mode and OPLS-3e power field and the above docking process was run in a flexible docking mode, which automatically generates conformations for each input ligand. The best-docked ligands are chosen based on MM-GBSA score using the Prime-MM-GBSA module of Schrödinger Maestro Suite 2020-2.

Statistical analysis

All experiments were performed in three technical replicates and at least two experimental repeats. *P* values were calculated using GraphPad Prism (version 9.0) by two-way ANOVA followed by the Tukey multiple comparisons test. ANOVA or Student *t* test was used for independent samples with normal distribution. Where distribution was not normal (assessed using Q–Q plots with the Wilk–Shapiro test of normality), either the Kruskal–Wallis or Wilcoxon rank sum test was used. Databases used for human data mining are from publicly available resources: cBioPortal and METABRIC data sets were used.

Results

HER2 mutations are associated with poor prognosis in ER^+ ILC

To identify recurrent HER2-activating mutations in ER^+ ILC and IDC metastatic breast cancer patients (MSK-IMPACT data set; ref. 13), we searched ER^+ ILC and IDC metastatic breast cancer sequencing studies. We found that 32 patient samples out of 284 (11.27%) ER^+ ILC patients have HER2 missense mutations or insertions, while only 32 patient samples out of 1,231 (2.60%) ER^+ IDC patients have HER2 missense mutations or insertions. The recurrent kinase domain (KD) mutation L755S was the dominant mutant allele in the metastatic breast cancer ILC subset, present in 11 patient samples, versus the extracellular domain (ECD) mutation S310F in three patient samples (**Fig. 1A**). In IDC metastatic breast cancer, recurrent kinase domain exon 20 insertions were found in 11 patient samples, and other activating KD mutations including L755S, V777L, and R678Q were also observed (**Fig. 1A**). In addition, the METABRIC cohort (22) showed L755S and L755 in-frame deletions in both ILC (4 patient samples) and IDC breast cancer (8 patient samples; Supplementary Fig. S2C).

To examine the clinical significance of recurrent HER2 mutations, we analyzed the prognostic effects of all HER2 mutations using ER^+ HER2 nonamplified METABRIC cohort on patient outcome and found that all HER2 mutations taken together are not associated with reduced OS as compared with all HER2 wild-type (HER2 WT) (Supplementary Fig. S1A). Next, we analyzed the prognostic effects of only four selected HER2 activating mutations (S310F, V777L, L755S, and Exon 20 ins/del) in the ER^+ HER2 nonamplified subset of the METABRIC cohort. We observed that patients with tumors harboring selected HER2-activating mutations (L755S, S310F, V777L, and Exon 20 ins/del) had significantly reduced OS compared with those with HER2 wild-type (HER2 WT; **Fig. 1B**). In order to study the prevalence of HER2 mutations in both ER^+ ILC and ER^+ IDC, we analyzed the sequencing results of METABRIC and MSK/IMPACT studies (13, 22) and compared the prevalence of HER2 mutations and HER2 amplification in the ER^+ subset. We noticed a significantly higher incidence of HER2 mutations in ILCs (9.65% in METABRIC and 11.27% in MSK/IMPACT) as opposed to IDCs (2.73% in METABRIC and 2.60% in MSK-IMPACT). In contrast, HER2 amplification was higher in IDC cases, with 5.68% (METABRIC) and 7.88% (MSK/IMPACT) as opposed to 0.87% (METABRIC) and 4.58% (MSK/IMPACT) in ILC patients, suggesting that HER2 mutations may be important pathogenic drivers in a subset of ER^+ ILC (**Fig. 1C**).

To comprehensively address the relationship between HER2 mutations and outcomes in ER^+ ILC as compared with ER^+ IDC, we analyzed METABRIC ER^+ ILC and IDC patients and compared their overall and breast cancer disease-specific survival probabilities. In line with a previously published report (23), we demonstrate that all HER2 mutations (Supplementary Fig. S1B and S1C) or selected (L775S and Exon 20 ins/del) HER2 mutations (Supplementary Fig. S1D) were associated with significantly worse overall or breast cancer disease-specific survival as compared with HER2 WT, but only in ER^+ ILC. Subsequently, we also investigated the prognostic significance of L755 alterations (L755S and L755_T759del) in ER^+ ILC. ILC patients harboring L755 alterations showed reduced OS compared with those

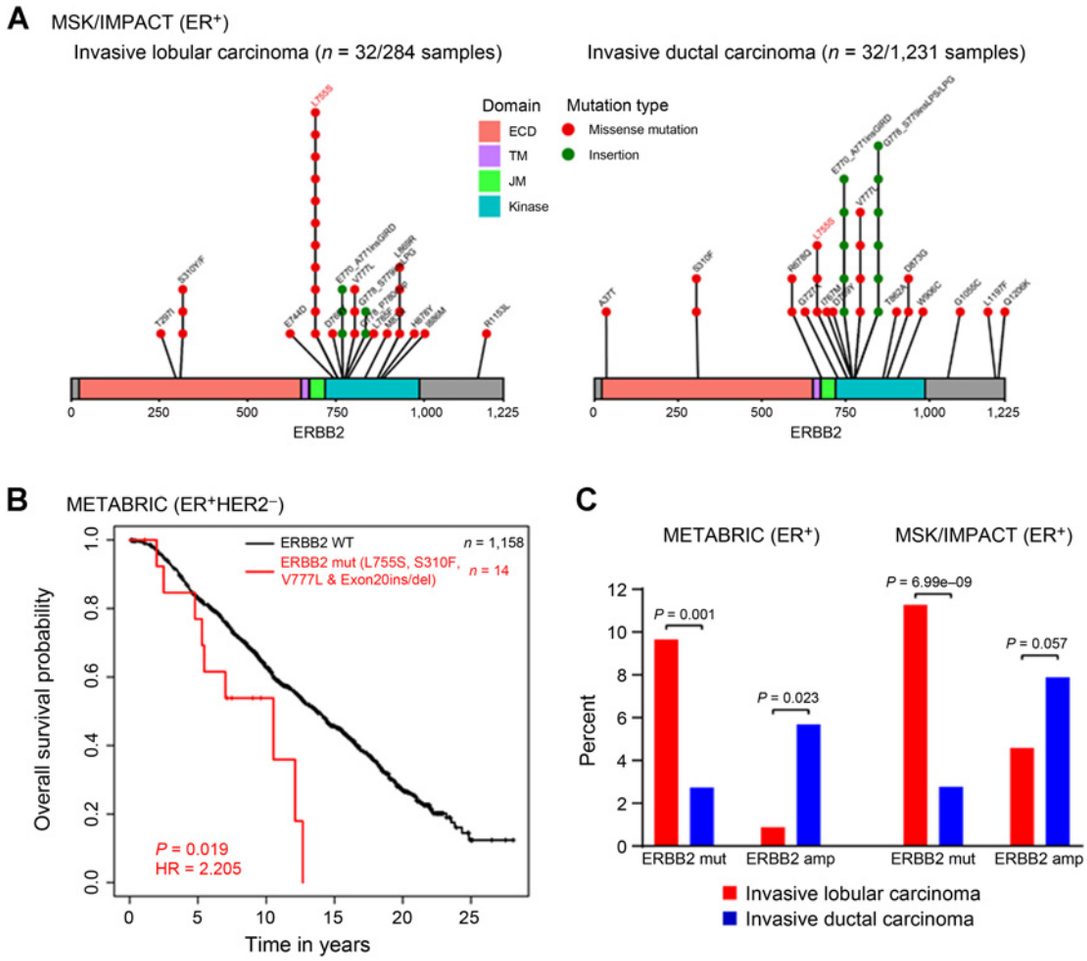

Figure 1.

HER2 mutations are significantly enriched in ILC as compared with IDC, in ER$^+$ primary and metastatic breast cancer. **A,** Lolliplot showing HER2 mutations identified from the MSK/IMPACT data set in ER$^+$/ILC and IDC. Three HER2-mutant patient samples (T297I, L755S, and L869R) harbor co-occurring HER2 amplification in ILC. Five HER2-mutant patient samples (E770_A771insGIRD, R678Q, V777L, V777L, and A37T) harbor co-occurring HER2 amplification in IDC. Two patient samples in ILC have more than one co-occurring mutation. One patient sample in IDC has more than one co-occurring mutation. **B,** Kaplan–Meier curves showing OS analysis of recurrent selected HER2 mutations (L755S, S310F, V777L, and Exon 20ins/del) in the ER$^+$ and HER2 nonamplified subsets of the METABRIC cohort. *P* value determined by the Wald test. HR, hazard ratio. **C,** The prevalence of HER2 mutations was examined in ILC and IDC using primary (METABRIC) and metastatic (MSK-IMPACT) ER$^+$ sequencing studies. The ILC subset shows 9.65% (METABRIC) and 11.27% (MSK/IMPACT) prevalence as opposed to 2.73% (METABRIC) and 2.60% (MSK/IMPACT) in the IDC subset. In addition, the prevalence of HER2 amplification was examined in ER$^+$ ILC and IDC cohorts. The ILC subset shows 0.87% (METABRIC) and 4.58% (MSK/IMPACT) prevalence as opposed to 5.68% (METABRIC) and 7.88% (MSK/IMPACT) in the IDC subset.

with HER2WT, suggesting that recurrent L755 alterations are associated with more aggressive ER$^+$ ILC disease biology (Supplementary Fig. S1E). We could not detect any difference in overall or breast cancer disease-specific survival in ER$^+$ IDC (Supplementary Fig. S2A and S2B), suggesting that HER2 mutations induce early relapse primarily in ER$^+$ ILC as compared with ER$^+$ IDC patients.

Allele-specific effect of HER2 mutations on endocrine therapy resistance, tumor growth, and multiorgan metastasis in ER$^+$ ILC cells

We analyzed the endogenous expression of total HER2 and E-cadherin in ER$^+$ lobular [MDA-MB-134 (MM134) and SUM44PE] and ER$^+$ ductal (MCF7, T47D, and ZR-75) cell lines and observed low endogenous total HER2 expression in MM134 lobular as compared with SUM44PE lobular and other ductal cell lines. As expected, we noticed the loss of E-cadherin in lobular cell lines as compared with ductal cell lines (Supplementary Fig. S3A; refs. 24, 25). We next validated the HER2 ectopic expression of HER2 WT or mutant (S310F and L755S) MM134 cells and compared it with the HER2-amplified BT474 cell line (Supplementary Fig. S3B). To study the effect of endocrine therapy response on cell growth, MM134 ILC parental cells or cells expressing HER2 WT or HER2 mutants (S310F or L755S) were grown under low-estrogen conditions (in charcoal-stripped serum phenol-red-free media) and treated in the presence or absence of estradiol (E2) or the selective ER degrader fulvestrant. Estrogen-independent growth was increased in cells expressing S310F and L755S as compared with HER2 WT cells. Upon treatment with E2, cell growth was further increased in L755S-expressing cells, but fulvestrant was not inhibitory, suggesting that L755S can induce fulvestrant resistance in ER$^+$ ILC (Supplementary Fig. S3C). Further, to study

the functional impact of HER2 mutations S310F and L755S on downstream kinase signaling, MM134 parental cells or cells expressing HER2 WT, S310F, or L755S were grown under low-estrogen conditions and treated in the presence or absence of fulvestrant for 24 hours. Cells were harvested, protein lysates were prepared, and expression of HER2 downstream signaling proteins was analyzed. The cells expressing HER2 S310F and L755S showed increased levels of phospho-Akt and phospho-p44/42 MAPK. As expected, we observed decreased ERα upon fulvestrant treatment. Further, we also observed moderate downregulation of ERα in HER2 WT cells, in line with previous reports (**Fig. 2A**; ref. 26). These results suggest that L755S may cause fulvestrant resistance by increasing constitutive HER2 downstream kinase signaling.

The ability of parental, HER2 WT, or HER2 mutants S310F and L755S to induce E2-independent growth was further tested *in vivo* by injecting these MM134 cell lines into the mammary fat pads of NSG mice. Mice were supplemented with E2 in water until the tumor size reached 250–400 mm^3. E2 was then withdrawn, and tumor growth was further monitored in the absence of E2. L755S-expressing cells continued to grow and form tumors even upon E2 withdrawal, whereas S310F-induced tumor growth remained stable upon E2 removal. Parental and WT tumors were relatively slow-growing even in the presence of E2 (**Fig. 2B**). Subsequently, we performed survival surgeries of L755S-bearing mice when tumors reached 800–1,000 mm^3 and monitored metastatic spread to secondary sites. These mice were euthanized ∼6 weeks following survival surgery, and lungs and ovaries were harvested. Hematoxylin and eosin and immunohistochemical (IHC) staining was carried out for phosphorylated HER2 (pHER2) and total ERα expression in the lungs and ovaries, revealing metastasis in L755S tumor-bearing mice upon E2 deprivation. Additionally, the

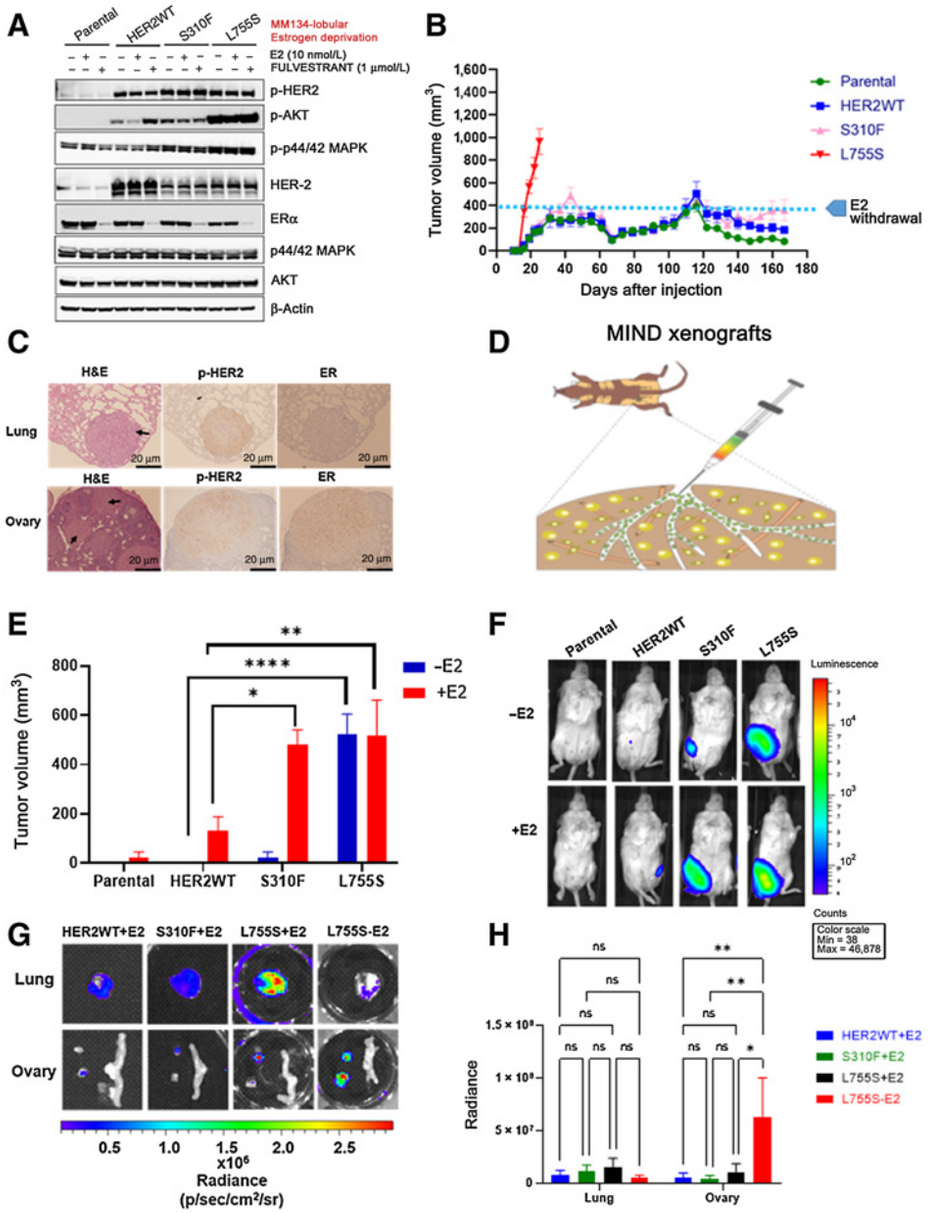

Figure 2.

Allele-specific estrogen-independent tumor growth and metastasis of HER2 mutations in ER^+ ILC. **A,** MM134 lobular parental cells or cells expressing HER2 WT or S310F or L755S were grown in low-estrogen conditions. The cells were treated in the presence or absence of fulvestrant or estradiol (E2) for 24 hours at the indicated concentrations and protein lysates were harvested. HER2 downstream signaling proteins were assessed by immunoblot analysis. **B,** MM134 parental cells or cells expressing HER2 WT or S310F or L755S were engrafted into mouse mammary fat pads in the presence of E2 until tumor size reached 250–400 mm^3. Subsequently, E2 was withdrawn and tumor growth was monitored. Each data point represents the mean tumor volume in $mm^3 \pm$ SEM, $n = 7$–8. **C,** L755S tumor-bearing mice from **Fig. 2B** were subjected to survival surgeries when the tumor volume reached 800–1,000 mm^3, the mice were euthanized, lungs and ovaries were harvested, and IHC was performed for p-HER2 and ERα. Scale bar, 20 μm. p-HER2 and ER staining was scored in these sections. Ovary p-HER2 (score: 3+), ER: positive 88% positive cells, lungs p-HER2 (score: +3), ER: negative 0% positive cells. H&E, hematoxylin and eosin. **D,** Schematic representation of MM134 HER2 L755S luciferase coexpressing cells used in the MIND xenograft model. **E,** MM134 parental cells or cells expressing HER2 WT or S310F or L755S were engrafted intraductally in the presence or absence of E2, and tumor growth was monitored. The data are plotted as mean of tumor volume in $mm^3 \pm$ SEM, $n = 5$. *, $P = 0.04$; **, $P = 0.004$; ***, $P < 0.0001$. **F,** Bioluminescence images of **E** on day 95. **G,** Representative bioluminescence *ex vivo* images of WT (+E2), S310F (+E2), L755S (+E2), and L755S (−E2). **H,** Quantification of the bioluminescence signal from **G**. *, $P = 0.01$; **, $P \leq 0.005$; ns, nonsignificant.

lung and ovary lesions stained positive for pHER2 and total ERα (**Fig. 2C**).

Next, to examine the effect of HER2 mutations S310F and L755S on tumor growth and metastatic spread within the epithelial microenvironment, we generated mammary intraductal (MIND) xenograft models (schematic, **Fig. 2D**; ref. 27). MM134 parental and HER2 WT, S310F, and L755S luciferase-expressing cells were injected into the mammary ducts of NSG mice in the presence or absence of E2 supplementation. L755S-expressing cells formed tumors in the absence or presence of E2 supplementation, similar to FP xenografts. However, HER2 WT and HER2 S310F cells formed tumors only in the presence of E2 supplementation and they never formed palpable tumors in the absence of E2 until 219 days, revealing that HER2 WT and HER2 S310F-induced tumor growth is E2 dependent (**Fig. 2E** and **F**). Mice were euthanized when the tumor volume reached 1,500 mm^3 and lungs and ovaries were harvested for *ex vivo* analysis using bioluminescence (BL) imaging. In the absence of E2, HER2 L755S bearing mice showed significant ovary metastasis as compared with HER2 WT and HER2 S310F. In the presence of E2, HER2 L755S and HER2 S310F mice exhibited metastasis in both lungs and ovaries, but this was not significant as compared with HER2 WT (**Fig. 2G** and **H**; **Table 1**). Additionally, IHC staining of ovary lesions from L755S mice was positive for pHER2 and total ERα (Supplementary Fig. S3D). Together, these findings reveal that HER2 L755S is sufficient to drive E2-independent mammary tumor growth and multiorgan metastasis in ER^+ ILC FP and MIND xenografts.

HER2 L755S-expressing tumors are resistant to neratinib and fulvestrant *in vivo*

To investigate the effect of HER2 mutations on *in vivo* tumor responses to fulvestrant and the HER2 TKI neratinib, we engrafted HER2 WT, S310F, and L755S MM134 cell lines into mouse mammary fat pads of NSG mice. Mice were supplemented with E2 until the tumor volume reached 300–400 mm^3. The HER2 WT and HER2 S310F mice were then randomized into six groups: vehicle, fulvestrant, or neratinib, with E2 withdrawal or continuation. We observed that tumor growth in mice bearing HER2 WT or S310F was highly sensitive to neratinib or fulvestrant in the presence or absence of E2 (Supplementary Fig. S4A and S4B). For L755S cells, E2 was withdrawn, and mice were randomized to receive vehicle, neratinib, or fulvestrant. Fulvestrant and neratinib as single agents did not affect tumor growth (Supplementary Fig. S4C). To complement our mouse xenograft data, we analyzed neratinib responses in clinical trials of ER^+ HER2-mutant breast cancers (9, 11, 20, 28) and found that patients harboring HER2 L755S had a higher incidence of progressive disease and lower incidence of complete response compared with patients harboring other HER2 mutations (S310F, exon 20 insertions, and other actionable KD mutations), thereby suggesting "allele-specific" neratinib responses in ER^+ breast cancer (**Table 2**).

Table 1. Lung and ovary positivity by IVIS, shown as a table from **Fig. 2G**.

Experimental Group	Lung positive by IVIS	Ovary positive by IVIS
WT+E2	5/7	2/7
S310+E2	2/5	2/5
L755S+E2	3/5	4/5
L755S-E2	1/4	4/4

Table 2. Allele-specific HER2-mutant responses to neratinib using ER^+ HER2-mutant breast cancer clinical trials data.

HER2 mutations	PD	SD	PR	CR
L755S/P	18	11	3	2
L755 alterations	1	1	2	
Exon 20 Ins	1	10	7	3
D769H/Y	2	6	1	1
L869R		1	4	
S310F	5	4	1	2
V8421		1		
V777L	9		2	

Abbreviations: CR, complete response; PD, progressive disease; PR, partial response; SD, stable disease.

(1) Total number of HER2-mutant breast cancer cases in Hyman et al. (ref. 9; neratinib as a monotherapy), 25 patients (20 ER^+ and 5 ER^-).

(2) Total number of HER2-mutant breast cancer cases in Smyth et al. (ref. 20; neratinib as a monotherapy), 34 patients (23 ER^+ and 11 ER^-).

(3) Total number of HER2-mutant breast cancer cases in Ma et al. (ref. 11; neratinib as a monotherapy), 22 patients (21 ER^+ and 1 ER^-).

(4) Total number of HER2-mutant breast cancer cases in Ma et al. [ref. 28; neratinib alone or neratinib + fulvestrant treated mixed cohort, 40 patients (including neratinib + fulvestrant = 24 patients; neratinib alone = 11 patients; ER^+ patients = 35; ER^- patients = 5].

The pan-HER drug poziotinib durably inhibits HER2 L755S-expressing cell viability *in vitro* and tumor growth *in vivo*

To compare the effects of pan-HER small-molecule inhibitors (neratinib, pyrotinib, and poziotinib) on cell growth, MM134 parental and HER2 WT, S310F, or L755S cells were treated with each drug under long-term low-estrogen conditions and monitored for cell viability using the CellTiter-Glo assay. Cell growth inhibition by all pan-HER small-molecule inhibitors was similar in parental, HER2 WT, and HER2 S310F cells, but poziotinib even at lower concentrations, 1 nmol/L, significantly reduced viability of HER2 L755S expressing cells (Supplementary Fig. S5A). To better understand this, we determined IC_{50} values for neratinib versus poziotinib. Neratinib reduced L755S cell viability with an IC_{50} value of 1.3 nmol/L, whereas poziotinib was more potent with an IC_{50} of 0.3 nmol/L (**Fig. 3A**). We also determined the IC_{50} values for tucatinib in both MM134 HER2 WT and HER2 L755S cells and observed that tucatinib reduced the viability of these cells with IC_{50} values of 117 nmol/L and 103 nmol/L, respectively (Supplementary Fig. S5B). We next tested the effect of neratinib or poziotinib on HER2 downstream kinase signaling. Neratinib and poziotinib at 10 nmol/L had a similar inhibitory effect on L755S induced pHER2 and the associated downstream signaling protein p-Akt, whereas in contrast 10 nmol/L neratinib was more effective than poziotinib in strongly inhibiting the p-p44/42 MAPK signaling (Supplementary Fig. S5C). A similar immunoblot analysis was done in HER2 L869R cells as well, and we observed that 10 nmol/L poziotinib was effective in inhibiting the pHER2 expression and its downstream signaling protein p-Akt; however, we observed no change in p-p44/42 MAPK signaling (Supplementary Fig. S5D). We also determined the IC_{50} values for both neratinib and poziotinib in MM134 HER2 L869R cells—neratinib and poziotinib reduced the viability of these cells with IC_{50} values of 107 nmol/L and 257 nmol/L, respectively (Supplementary Fig. S5E). Further, we also confirmed the constitutive phosphorylation of HER2 in CRISPR KI SUM44PE V777L (homozygous) and L755S (heterozygous) cells. Upon treatment with neratinib or poziotinib, poziotinib was effective in inhibiting the pHER2 expression at 10 nmol/L concentration in both V777L and L755S cells (Supplementary Fig. S6A). The CRISPR KI SUM44PE

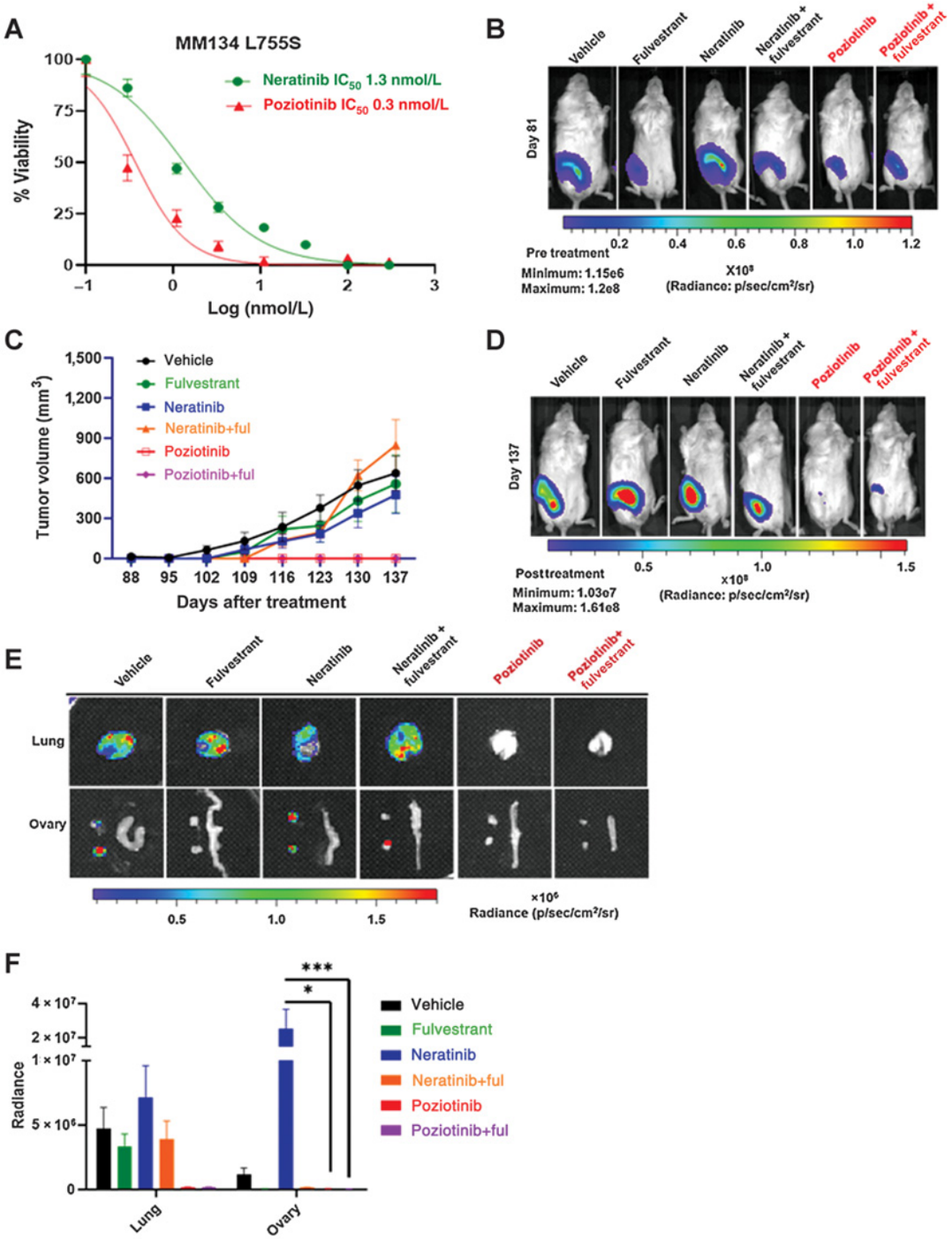

Figure 3.

ER$^+$ ILC L755S is resistant to neratinib but sensitive to poziotinib. **A,** Dose-response curves for HER2 WT and HER2 L755S cells grown in E2-deprived media, to which increasing concentrations of neratinib and poziotinib were added twice a week for 4 weeks. **B,** MM134 L755S cells were engrafted into mouse mammary ducts in the absence of E2 until tumor size reached 4.5×10^8 radiance. Bioluminescence images on day 81 (pre-randomization). **C,** Subsequently, the mice were randomized in the presence of vehicle or fulvestrant (250 mg/kg body weight of mice) or neratinib chow (40 mg/kg) or poziotinib chow (10 mg/kg). Tumor volume was measured by calipers, and tumor growth was monitored. The data are plotted as mean tumor volume in $mm^3 \pm$ SEM, $n = 7$–8. The significance (P value) was calculated on day 56 post drug treatment or day 137 post injection, vehicle vs. poziotinib <0.0001, vehicle vs. poziotinib + fulvestrant <0.0001, neratinib vs. poziotinib <0.0001, neratinib vs. poziotinib + fulvestrant <0.0001, neratinib + fulvestrant vs. poziotinib < 0.0001, vehicle vs. neratinib N.S, and vehicle vs. neratinib + fulvestrant N.S. (N.S., no significance). **D,** Bioluminescence images on day 137 (endpoint). **E,** Representative bioluminescence *ex vivo* images of lung and ovaries of L755S mice in the presence or absence of indicated drugs. **F,** Bioluminescence radiance quantification of lungs and ovaries from **E**. *, $P = 0.01$; ***, $P = 0.0003$.

V777L and L755S clones were sequence verified (Supplementary Fig. S6B)

To study the *in vivo* effect of neratinib, poziotinib, or fulvestrant, alone or in combination, on tumor growth and multiorgan metastasis, we generated luciferase-expressing MM134 HER2 L755S MIND xenografts in the absence of E2 supplementation and subjected the mice to the indicated drug treatments until tumor radiance reached 4.5×10^8 by BL imaging (**Fig. 3B**). The mice were monitored for intraductal primary tumor growth by BL imaging, and tumor volume was measured at the orthotopic site of injection (**Fig. 3C**). Upon treatment with neratinib or fulvestrant or neratinib + fulvestrant, the primary tumors continued to grow, and the tumor growth was similar to vehicle-treated mice. In contrast, poziotinib alone or in combination with fulvestrant durably inhibited tumor growth throughout the course of 7 weeks (long term) of drug treatment (**Fig. 3D**; Supplementary Fig. S7A). Collectively, these data indicate that poziotinib as a single agent or in combination with fulvestrant may be efficacious in reducing ER^+ L755S-driven tumorigenesis in the ILC mouse model.

Poziotinib abolishes lung and ovary metastasis, whereas neratinib is inefficient in reducing metastatic burden

To further assess the efficacy of poziotinib in the metastatic setting, we analyzed by *ex vivo* BL imaging the lungs and ovaries from L755S-bearing mice that had been treated for 7 weeks (**Fig. 3E**). Surprisingly, in our experimental model, neratinib was ineffective in reducing ovary metastasis. However, mice treated with poziotinib alone or in combination with fulvestrant had no evidence of lung or ovary metastasis (**Fig. 3F**; **Table 3**). We also monitored total body weight of the mice bearing tumors during the course of drug treatment and observed no significant loss of body weight with the drug treatment (Supplementary Fig. S8A).

To analyze the short term *in vivo* efficacy of poziotinib, we generated HER2 L755S MIND xenografts (MM134) and monitored primary tumors until radiance reached 1×10^9 by BL imaging. Then we randomized the mice and treated with vehicle or poziotinib. Following only 3 weeks of treatment (short term), we observed a significant reduction of primary tumor and ovary metastasis burden in poziotinib-treated mice, although we did not observe a significant reduction in lung metastasis burden in these mice (Supplementary Fig. S7B–S7D). We analyzed signaling of these tumors by immunoblotting and found that poziotinib reduced the levels of phospho-HER2, phospho-Akt, phospho-p44/42 MAPK, phospho-mTOR, and phospho-S6, suggesting that poziotinib can inhibit L755S-induced orthotopic tumor growth, oncogenic signaling, and ovary metastasis even with a short duration of treatment (Supplementary Fig. S7E). Taken together, these data clearly suggest that poziotinib may be useful for the treatment of HER2-mutant metastatic ILC.

Table 3. Lung and ovary positivity by IVIS shown as a table from **Fig. 3E**.

Experimental group	Lung positive by IVIS	Ovary positive by IVIS
Vehicle	5/8	6/8
Fulvestrant	6/8	0/8
Neratinib	5/8	5/8
Neratinib + fulvestrant	7/7	2/7
Poziotinib	0/3	0/3
Poziotinib + fulvestrant	0/7	0/7

Poziotinib durably inhibits tumor growth of the MCF7 L755S xenografts as well as the ER^+ IDC HCI-003 PDX model (harboring activating exon 20 $HER2^{G778\_P780\ dup}$ insertion)

To analyze the effect of pan-HER inhibitors in ER^+ IDC *in vitro* models, we performed dose-response studies in MCF7 L755S cells and observed cell growth inhibition with IC_{50} values of 65.4 nmol/L for neratinib, 2.1 nmol/L for poziotinib, 72 nmol/L for tucatinib, and 12.6 nmol/L for pyrotinib (**Fig. 4A**; Supplementary Fig. S10A). We next tested the effect of neratinib or poziotinib on HER2 downstream kinase signaling. Neratinib and poziotinib at 10 nmol/L had a similar inhibitory effect on L755S-induced pHER2 and the associated downstream signaling protein p-Akt, while in contrast 10 nmol/L neratinib was more effective than poziotinib in strongly inhibiting p-p44/42 MAPK signaling (Supplementary Fig. S10B). Also, in MCF-L755S KI (16) cells we observed higher total HER2 expression upon estrogen deprivation. This may be due to the HER2 receptor stabilization on the membrane upon estrogen deprivation.

We next sought to assess the efficacy of poziotinib in *in vivo* models of ER^+ HER2-mutant IDC. We generated an MCF7-L755S KI xenograft mouse model as previously reported (29). The ER^+ IDC PDX HCI-003 (30) naturally harbors an activating $HER2^{G778\_P780\ dup}$ and a concurrent PIK3CA H1074R mutation, known to potently activate PI3K signaling (31–33). We treated mice bearing MCF7 L755S MIND xenografts (in the absence of E2 supplementation) or orthotopic HCI-003 tumors (in the presence of E2 supplementation) with pan-HER inhibitors neratinib or poziotinib alone or in combination with fulvestrant. As we observed earlier in our MM134 HER2 L755S expressing MIND xenografts, neratinib, fulvestrant, and the combination had no effect on HCI-003 PDX tumor growth. However, poziotinib alone or combined with fulvestrant durably inhibited tumor growth in both the MCF7-L755S KI and HCI-003 PDX models (**Fig. 4B** and **C**). The total body weight of the mice was monitored during the course of drug treatment, and we observed no significant loss of body weight with the drug treatment (Supplementary Fig. S8B and S8C). Collectively, these results provide a strong preclinical rationale for poziotinib as a new treatment strategy for ER^+ HER2-mutant IDC.

Structural modeling of HER2 L755S explains preferential affinity for poziotinib

We conducted protein structure modeling of human HER2 L755 or S755 bound to neratinib and poziotinib, using the X-ray crystal structure of the KD of HER2 (PDB#3PP0; ref. 34). The HER2 kinase is predicted to adopt different conformations when bound by neratinib or poziotinib, which both have covalent binding modes that project deeply into the substrate-binding pocket of the HER2. The L755S (S775) mutation reduces the volume of the drug-binding pocket, which is predicted to limit the binding of drugs such as neratinib with larger terminal groups oriented toward the α-C helix. In contrast, due to the terminal halogenated benzene group of poziotinib, it can bind deeply within the hydrophobic cleft created by the L755S mutation. This interaction of the terminal benzene group with the hydrophobic cleft results in the alignment of the quinazoline core with residues at the back of the drug-binding pocket, maintaining receptor binding. S755 has enhanced poziotinib binding compared with L755 due to its binding with the neighboring R756. The lower binding energy score for L755S binding to poziotinib showed higher proximity and tighter binding as compared with WT (Supplementary Fig. S9A–S9F). Based on these studies, HER2 S755 is predicted to facilitate poziotinib binding at 2.7 Å distance as opposed to 10.2 Å for L755. The glide docking was also performed using the putative active site of HER2

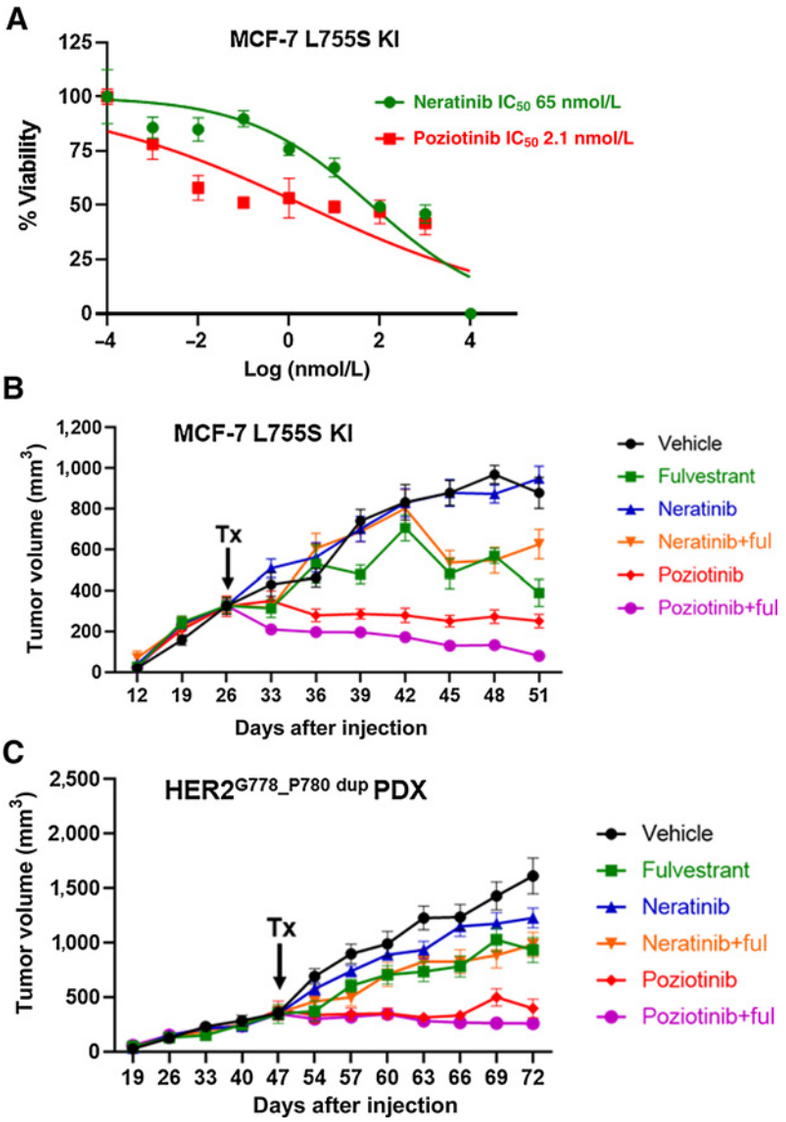

Figure 4.

ER$^+$ IDC HCI-003 PDX and ER$^+$ IDC MCF7-L755S KI *in vivo* models display resistance to neratinib but are sensitive to poziotinib alone or in combination with fulvestrant. **A,** Dose-response curves for MCF7-L755S KI cells grown in E2-deprived media, to which increasing concentrations of neratinib and poziotinib were added twice a week for 4 weeks. **B** and **C,** MCF7-L755S KI cells (**B**) or HCI-003 tumors (**C**) were engrafted into mouse mammary fat pads in the presence of E2 until tumor size reached 300–400 mm^3. Subsequently, the E2 supplementation was withdrawn in **B**, but was continued in **C**. The mice were randomized in the presence of vehicle or fulvestrant (250 mg/kg/body weight of mice) or neratinib chow (40 mg/kg) or poziotinib chow (10 mg/kg). Tumor volume was measured. The data are plotted as mean tumor volume in mm^3 ± SEM, $n = 5$–8. The significance (P value) of MCF7-L755S KI (**B**) was calculated on day 51, vehicle vs. poziotinib, <0.0001; vehicle vs. poziotinib + fulvestrant, <0.0001; poziotinib vs. neratinib, <0.0001; vehicle vs. neratinib, no significance; vehicle vs. neratinib + fulvestrant, 0.007; vehicle vs. fulvestrant, <0.0001. The significance (P value) of HCI-003 (**C**) was calculated on day 72, vehicle vs. poziotinib, <0.0001; vehicle vs. poziotinib + fulvestrant, <0.0001; poziotinib vs. neratinib, <0.0001; vehicle vs. neratinib, 0.002; and vehicle vs. neratinib + fulvestrant, <0.0001.

(3PP0); in this case, it was the ligand 03Q (IC_{50} = 11 nmol/L). The MM-GBSA binding energy again correlates with the initial trend, where it shows tighter binding with S755 when compared with L755, indicating that the point mutation of S755 led to more affinity toward poziotinib (Supplementary Fig. S9G and S9H). Together, these data suggest that the increased antitumor activity of poziotinib may be due to its closer binding proximity to S755.

Poziotinib inhibits Akt–mTOR signaling

We conducted RNA sequencing of MM134 cells expressing HER2 WT or L755S grown in low-estrogen conditions, followed by GSEA to identify altered gene-expression pathways in L755S cells. mTOR (also called MTORC1) signaling was the top significantly upregulated pathway in HER2 L755S cells (**Fig. 5A** and **B**). We then assessed mTOR activation in HER2 WT and L755S-expressing cells treated with neratinib or poziotinib. Poziotinib (10 nmol/L) but not neratinib (10 nmol/L) potently inhibited phospho-HER2, phospho-Akt, phospho-mTOR, and its substrate phospho-S6 in HER2 L755S-expressing cells (**Fig. 5C**; Supplementary Fig. S5C). We confirmed the inhibition of phospho-HER2, phospho-Akt, phospho-p44/42 MAPK, phospho-mTOR, and phospho-S6 in MCF7 L755S KI xenograft tumors obtained from **Fig. 4B** (**Fig. 5D**). Collectively, these data show that poziotinib potently inhibits primary tumor growth, multiorgan metastasis, and mTOR pathway activation. A schematic representation of the mechanism describing the efficacy of poziotinib in inhibiting HER2 L755S-induced tumor growth and metastasis is shown in **Fig. 5E**.

Discussion

Our observation of HER2 activating mutations as a therapeutic target in ER$^+$ breast and colorectal cancers (6, 10) led to ER$^+$ breast cancer clinical trials (NCT01670877; ref. 11) and SUMMIT basket trials across 21 different cancer types (NCT01953926; refs. 9, 20). In both of these trials, the response to the pan-HER inhibitor neratinib as a single agent was highly varied across different cancer types, with frequent early progression. Further, neratinib in combination with fulvestrant and trastuzumab was shown to be highly effective in HER2-

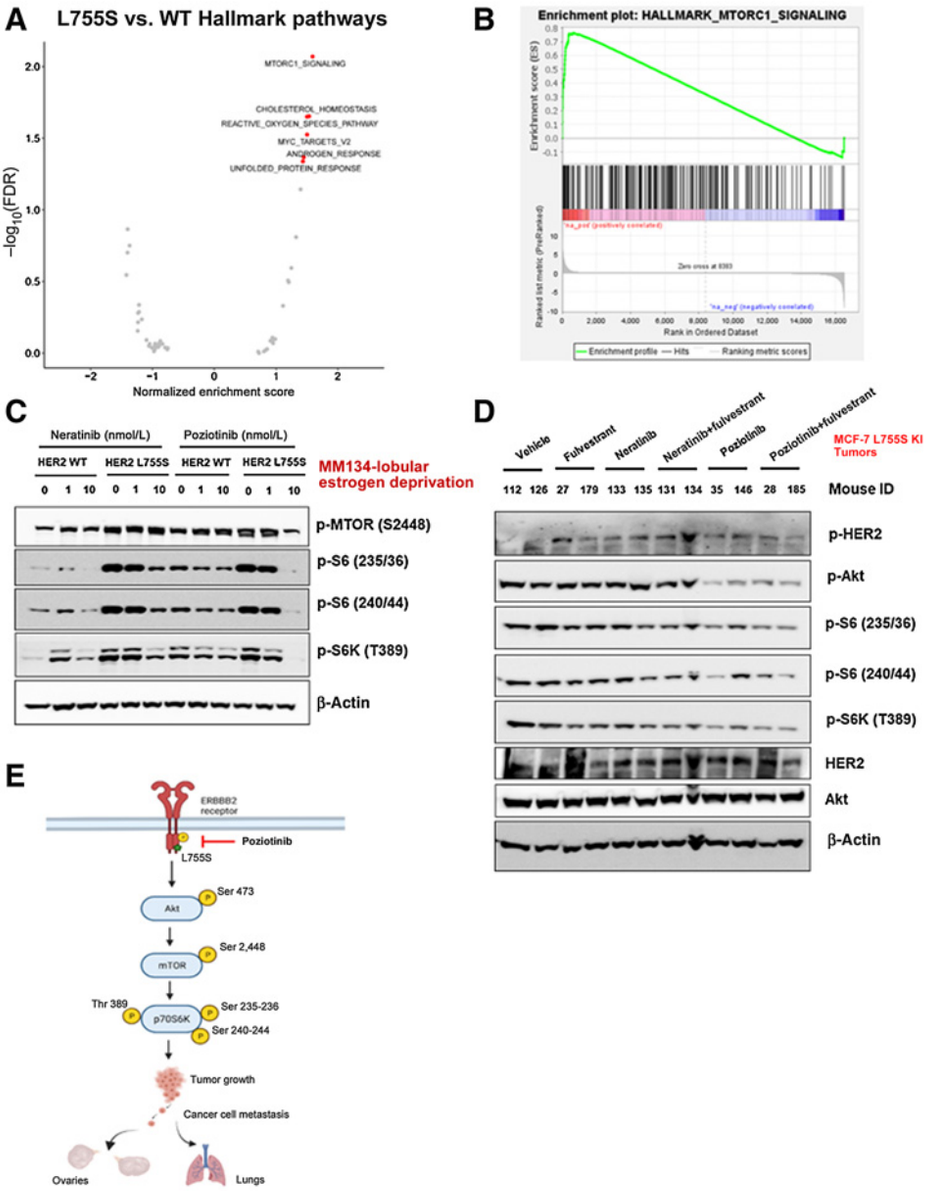

Figure 5.

HER2 mutations activate the HER2–mTOR signaling axis and may be associated with neratinib or fulvestrant resistance, yet poziotinib treatment alone inhibits the HER2–mTOR signaling axis. **A,** MM134 HER2 WT or L755S cells were grown in low-estrogen conditions and subjected to RNA sequencing analysis. GSEA of the top upregulated and downregulated genes in L755S cells as compared with HER2 WT cells identified the mTOR signaling pathway as the most significantly enriched pathway in L755S cells. **B,** Gene enrichment pathway analysis of RNA sequencing data from **A** was performed. Normalized enrichment score (NES) for the mTOR pathway is 1.59 and false discovery rate *q* value is 0.009. **C,** MM134 HER2 WT or L755S cells grown in low-estrogen conditions were treated with neratinib or poziotinib for 4 hours at the indicated concentrations. The cells were harvested and protein lysates were subjected to immunoblotting analysis for phospho-mTOR and its downstream substrate phospho-S6; protein expression. **D,** MCF7-L755S KI tumors were harvested from **Fig. 4B**, and protein lysates were subjected to immunoblot analysis for phospho-HER2, phospho-Akt, phospho-mTOR, and phospho-S6 protein expression. **E,** Schematic representation of mechanistic link describing poziotinib efficacy in inhibiting tumor growth and metastasis.

mutant ER$^+$ metastatic breast cancer (28). Thus, identifying HER2-mutant-specific effects on endocrine resistance, neratinib resistance, and multiorgan metastasis, in distinct histologic subtypes of ER$^+$ breast cancer, is of paramount importance if therapy directed against HER2 mutations is to advance.

In line with previous observations (23), we show that HER2 mutations are highly enriched in ER$^+$ primary and metastatic ILC but not IDC. The ER$^+$ HER2 nonamplified ILC patients harboring HER2 mutations have significantly shorter overall and disease-specific survival than patients harboring HER2 WT, as shown previously (35). In this study, ER$^+$ ILC patients harboring the L755 alterations (L755S and L755_T759del) showed significantly worse OS than HER2 WT ILC patients, suggesting that L755 alterations are unique pathogenic drivers in ER$^+$ ILC. These findings are consistent with other recent reports and suggest that the frequency of HER2 mutations is approximately 5%–26% and that L755S is a recurrent mutation in ILC (14, 18, 19). However, the HER2-mutant patient numbers are low in the primary METABRIC breast cancer data set, where we have a clinical follow-up, and the future studies will investigate the impact of ER$^+$ ILC and IDC HER2-mutant alleles on patient outcomes using larger ER$^+$ metastatic breast cancer cohorts. Existing literature has shown L755S to be a lapatinib-resistant mutation (36). In fact, recent phase II Mut HER2 neratinib trial data support our conclusions that neratinib as a single agent was effective in patients with lobular histology, though lobular patients harboring recurrent L755 alterations were associated with less clinical efficacy (28).

The functional impact of HER2 mutations on therapy-induced resistance and metastasis has not yet been evaluated. Our *in vivo* studies revealed that L755S promotes E2-independent tumor growth and resistance to fulvestrant and neratinib. In contrast, S310F-expressing cells remain E2-dependent and sensitive to fulvestrant and neratinib treatment. Using clinically relevant MIND xenografts, we

observed that HER2 L755S-expressing tumors displayed increased ovary metastasis in an E2-independent manner. These findings support other existing reports that, among metastatic breast cancer patients with ovarian metastasis, ILC patients have earlier relapses than IDC patients (37). The spread of ILC tumors to distant sites including ovaries, the gastrointestinal (GI) tract, and lungs makes this disease difficult to detect during initial and subsequent relapse diagnosis (37, 38). These findings are similar to the effect of allele-specific ESR1 mutations on endocrine therapy response and metastasis in ER^+ IDC (39, 40).

We compared the effects of pan-HER inhibitors on HER2-mutant cell growth and found that poziotinib was more effective in inhibiting L755S-induced growth than neratinib or pyrotinib even at lower concentrations (1 nmol/L). Although both neratinib and poziotinib were highly effective against S310F and HER2 WT-expressing cells, only poziotinib potently inhibited L755S-induced cell growth *in vitro* and *in vivo*. We confirmed these findings in a total of three independent *in vivo* models of ER^+ HER2-mutant breast cancer, including an ER^+ PDX (HCI-003) naturally harboring an exon 20 activating $HER2^{G778\_P780dup}$ mutation. Furthermore, poziotinib potently inhibited multiorgan metastasis in mice bearing HER2 L755S-expressing tumors. These results are in line with previous reports suggesting that poziotinib has higher antitumor activity than neratinib in CW-2 colorectal cancer cell xenografts harboring the L755S mutation. In addition, in this same study, MCF-10A breast epithelial cells ectopically expressing HER2 mutations were also shown to be more sensitive to poziotinib than to neratinib (41). The preclinical and clinical activity of poziotinib has already been evaluated in patients harboring recurrent HER2 exon 20 insertions in metastatic non–small cell lung cancer (NSCLC; refs. 41, 42). We also observed cell growth inhibition with tucatinib in our MM134 L755S model at a relatively higher concentration, with IC_{50} values of 103 and 0.3 nmol/L for tucatinib and poziotinib, respectively. The data presented in our study suggest that poziotinib has broader therapeutic implications beyond metastatic NSCLC (41) and refractory HER2-positive breast cancer (43). Poziotinib-associated clinical toxicity in NSCLC patients has already been documented (44).

In line with our poziotinib antitumor activity data, we speculate by structural modeling that poziotinib binds to HER2 with closer proximity to S755 as compared with L755. Therefore, differential drug-binding proximity on HER2 mutants is a possible explanation for different allele-specific therapeutic responses. The rigid docking studies performed here do not consider conformational changes of HER2 L755S or distribution in the active conformation. To our understanding, the Molecular Dynamics (MD) simulations need to be performed further to gain a better understanding of poziotinib–L755S proximity.

Indeed, recent reports suggest that the smaller drug-binding pocket of the recurrent HER2 exon 20 insertion and L755P mutants may be an important contributor to the higher potency of the smaller quinazoline-based TKIs poziotinib and afatinib (41). Poziotinib caused durable tumor and multiorgan metastasis inhibition and reduced mTOR activation potently. These data are consistent with other reports of the mTOR axis as a therapeutic vulnerability in ER^+ HER2-mutant breast cancer (45, 46).

In addition, the HCI-003 PDX model harboring a co-occurring pathogenic PIK3CA H1047R mutation showed tumor regression upon treatment with poziotinib alone or in combination with fulvestrant, suggesting that poziotinib may have antitumor activity in patients harboring co-occurring HER2 and PIK3CA mutations. Based on our preclinical findings described above, we propose that poziotinib is worthy of clinical investigation in a subset of ER^+ metastatic breast cancer harboring HER2 mutations. Further studies are warranted to evaluate poziotinib as a therapeutic agent in additional tumor types.

Authors' Disclosures

L.E. Dobrolecki reports personal fees from StemMed, Ltd. outside the submitted work. C. Yates reports personal fees from Riptide Biosciences and QED Therapeutics outside the submitted work. B. Lim reports other support from Puma Biotechnology, Genentech, and Merck outside the submitted work. M.J. Ellis reports grants from CPRIT and McNair Medical Foundation during the conduct of the study; personal fees from AstraZeneca outside the submitted work; in addition, M.J. Ellis has a patent for PAM50 issued, licensed, and with royalties paid from Veracyte. S.M. Kavuri reports other support from NeoZenome Therapeutics Inc. outside the submitted work. No disclosures were reported by the other authors.

Authors' Contributions

R. Kalra: Conceptualization, data curation, software, formal analysis, validation, investigation, visualization, methodology, writing–original draft, project administration, writing–review and editing. **C. Chen:** Resources, data curation, software, formal analysis, validation, investigation, visualization, methodology. **J. Wang:** Resources, data curation, software, formal analysis, methodology. **A. Salam:** Data curation, software. **L.E. Dobrolecki:** Resources, methodology. **A. Lewis:** Resources, methodology. **C. Sallas:** Resources, methodology. **C.C. Yates:** Resources, methodology. **C. Gutierrez:** Data curation, formal analysis, methodology. **B. Karanam:** Data curation, methodology. **M. Anurag:** Resources, data curation, validation, methodology, writing–review and editing. **B. Lim:** Validation, investigation, visualization, methodology, project administration, writing–review and editing. **M.J. Ellis:** Conceptualization, funding acquisition, validation, investigation, visualization, writing–original draft, project administration, writing–review and editing. **S.M. Kavuri:** Conceptualization, resources, data curation, software, formal analysis, supervision, funding acquisition, validation, investigation, visualization, methodology, writing–original draft, project administration, writing–review and editing.

Acknowledgments

Research work in this study was funded by Susan G. Komen (CCR16380599 to S.M. Kavuri) and the Department of Defense (W81XWH-18-1-0040 and W81XWH-18-1-0084 to S.M. Kavuri), a Susan G. Komen Promise grant (PG12220321 to MJE), a Cancer Prevention and Research Institute of Texas (CPRIT) Recruitment of Established Investigators award (RR140033 to M.J. Ellis), a SPORE grant (P50CA186784-06 to M.J. Ellis), and an NCI SPORE Career Enhancement award to M. Anurag (part of P50 CA186784-06). The authors acknowledge the Patient-derived Xenograft and Advanced *in vivo* Models core (funded by P30 Cancer Center Support Grant NCI-CA125123 and CPRIT Core Facilities Support Grant RP170691) for their help in the experiments. Further support was provided by NIH grant (1R41CA257110-01) to B. Karanam, and DOD/PCRP PC190741 to C.C. Yates and B. Karanam. The authors would like to thank Drs. Gloria Echeverria, Charles Foulds, Xiang Zhang, and Gary Chamness for critical reading of the manuscript. They would like to thank Dr. Ben Ho Park (Vanderbilt University Medical Center) for providing MCF7 breast cancer cells with KI HER2 WT or the L755S HER2-activating mutation. The authors also thank Drs. Jeffrey Rosen, Eric Chang, Svasti Haricharan, and Michael T. Lewis for valuable scientific discussions. They would also like to thank patient advocate Josh Newby for helpful discussions. The authors thank Vivekanand Rangaswamy for assistance with **Fig. 2D**, Sufeng Mao (Breast Center Pathology Core, Baylor College of Medicine) for helping them in preparation of the IHC slides, and Jun Xu (Cell-Based Assay Screening Service Core, Baylor College of Medicine) for helping them in generating SUM44PE CRISPR KI cells. The authors would also like to thank Dr. Jin Wang for advising them on the glide docking studies and the Genomic and RNA Profiling Core (GARP) at Baylor College of Medicine for constructing libraries for RNA sequencing.

The costs of publication of this article were defrayed in part by the payment of page charges. This article must therefore be hereby marked *advertisement* in accordance with 18 U.S.C. Section 1734 solely to indicate this fact.

Note

Supplementary data for this article are available at Cancer Research Online (http://cancerres.aacrjournals.org/).

Received September 13, 2021; revised April 1, 2022; accepted June 14, 2022; published first June 23, 2022.

References

1. Pernas S, Tolaney SM. HER2-positive breast cancer: new therapeutic frontiers and overcoming resistance. Ther Adv Med Oncol 2019;11:1–16.
2. Cancer Genome Atlas N. Comprehensive molecular characterization of human colon and rectal cancer. Nature 2012;487:330–7.
3. Cancer Genome Atlas N. Comprehensive molecular portraits of human breast tumours. Nature 2012;490:61–70.
4. Cancer Genome Atlas Research N. Comprehensive molecular characterization of urothelial bladder carcinoma. Nature 2014;507:315–22.
5. Ben-Baruch NE, Bose R, Kavuri SM, Ma CX, Ellis MJ. HER2-mutated breast cancer responds to treatment with single-agent neratinib, a second-generation HER2/EGFR tyrosine kinase inhibitor. J Natl Compr Canc Netw 2015;13:1061–4.
6. Bose R, Kavuri SM, Searleman AC, Shen W, Shen D, Koboldt DC, et al. Activating HER2 mutations in HER2 gene amplification negative breast cancer. Cancer Discov 2013;3:224–37.
7. Croessmann S, Formisano L, Kinch LN, Gonzalez-Ericsson PI, Sudhan DR, Nagy RJ, et al. Combined blockade of activating ERBB2 mutations and ER results in synthetic lethality of ER+/HER2 mutant breast cancer. Clin Cancer Res 2019;25:277–89.
8. Goncalves R, Warner WA, Luo J, Ellis MJ. New concepts in breast cancer genomics and genetics. Breast Cancer Res 2014;16:460.
9. Hyman DM, Piha-Paul SA, Won H, Rodon J, Saura C, Shapiro GI, et al. HER kinase inhibition in patients with HER2- and HER3-mutant cancers. Nature 2018;554:189–94.
10. Kavuri SM, Jain N, Galimi F, Cottino F, Leto SM, Migliardi G, et al. HER2 activating mutations are targets for colorectal cancer treatment. Cancer Discov 2015;5:832–41.
11. Ma CX, Bose R, Gao F, Freedman RA, Telli ML, Kimmick G, et al. Neratinib efficacy and circulating tumor DNA detection of HER2 mutations in HER2 nonamplified metastatic breast cancer. Clin Cancer Res 2017;23:5687–95.
12. Nayar U, Cohen O, Kapstad C, Cuoco MS, Waks AG, Wander SA, et al. Acquired HER2 mutations in ER(+) metastatic breast cancer confer resistance to estrogen receptor-directed therapies. Nat Genet 2019;51:207–16.
13. Razavi P, Chang MT, Xu G, Bandlamudi C, Ross DS, Vasan N, et al. The genomic landscape of endocrine-resistant advanced breast cancers. Cancer Cell 2018;34:427–38.
14. Rosa-Rosa JM, Caniego-Casas T, Leskela S, Cristobal E, Gonzalez-Martinez S, Moreno-Moreno E, et al. High frequency of ERBB2 activating mutations in invasive lobular breast carcinoma with pleomorphic features. Cancers 2019;11:74.
15. Weigelt B, Reis-Filho JS. Activating mutations in HER2: neu opportunities and neu challenges. Cancer Discov 2013;3:145–7.
16. Zabransky DJ, Yankaskas CL, Cochran RL, Wong HY, Croessmann S, Chu D, et al. HER2 missense mutations have distinct effects on oncogenic signaling and migration. Proc Natl Acad Sci U S A 2015;112:E6205–14.
17. O'Leary B, Cutts RJ, Liu Y, Hrebien S, Huang X, Fenwick K, et al. The genetic landscape and clonal evolution of breast cancer resistance to palbociclib plus fulvestrant in the PALOMA-3 trial. Cancer Discov 2018;8:1390–403.
18. Desmedt C, Zoppoli G, Gundem G, Pruneri G, Larsimont D, Fornili M, et al. Genomic characterization of primary invasive lobular breast cancer. J Clin Oncol 2016;34:1872–81.
19. Zhu S, Ward BM, Yu J, Matthew-Onabanjo AN, Janusis J, Hsieh CC, et al. IRS2 mutations linked to invasion in pleomorphic invasive lobular carcinoma. JCI Insight 2018;3:e97398.
20. Smyth LM, Piha-Paul SA, Won HH, Schram AM, Saura C, Loi S, et al. Efficacy and determinants of response to HER kinase inhibition in HER2-mutant metastatic breast cancer. Cancer Discov 2020;10:198–213.
21. Kavuri SM, Geserick P, Berg D, Dimitrova DP, Feoktistova M, Siegmund D, et al. Cellular FLICE-inhibitory protein (cFLIP) isoforms block CD95- and TRAIL death receptor-induced gene induction irrespective of processing of caspase-8 or cFLIP in the death-inducing signaling complex. J Biol Chem 2011;286:16631–46.
22. Curtis C, Shah SP, Chin SF, Turashvili G, Rueda OM, Dunning MJ, et al. The genomic and transcriptomic architecture of 2,000 breast tumours reveals novel subgroups. Nature 2012;486:346–52.
23. Kurozumi S, Alsaleem M, Monteiro CJ, Bhardwaj K, Joosten SEP, Fujii T, et al. Targetable ERBB2 mutation status is an independent marker of adverse prognosis in estrogen receptor positive, ERBB2 nonamplified primary lobular breast carcinoma: a retrospective in silico analysis of public datasets. Breast Cancer Res 2020;22:85.
24. Sikora MJ, Cooper KL, Bahreini A, Luthra S, Wang G, Chandran UR, et al. Invasive lobular carcinoma cell lines are characterized by unique estrogen-mediated gene expression patterns and altered tamoxifen response. Cancer Res 2014;74:1463–74.
25. Tasdemir N, Ding K, Savariau L, Levine KM, Du T, Elangovan A, et al. Proteomic and transcriptomic profiling identifies mediators of anchorage-independent growth and roles of inhibitor of differentiation proteins in invasive lobular carcinoma. Sci Rep 2020;10:11487.
26. Gutierrez C, Schiff R. HER2: biology, detection, and clinical implications. Arch Pathol Lab Med 2011;135:55–62.
27. Sflomos G, Dormoy V, Metsalu T, Jeitziner R, Battista L, Scabia V, et al. A preclinical model for ERalpha-positive breast cancer points to the epithelial microenvironment as determinant of luminal phenotype and hormone response. Cancer Cell 2016;29:407–22.
28. Ma CX, Luo J, Freedman RA, Pluard TJ, Nangia JR, Lu J, et al. The phase II MutHER study of neratinib alone and in combination with fulvestrant in HER2-mutated, non-amplified metastatic breast cancer. Clin Cancer Res 2022;28:1258–67.
29. Punturi NB, Seker S, Devarakonda V, Mazumder A, Kalra R, Chen CH, et al. Mismatch repair deficiency predicts response to HER2 blockade in HER2-negative breast cancer. Nat Commun 2021;12:2940.
30. DeRose YS, Wang G, Lin YC, Bernard PS, Buys SS, Ebbert MT, et al. Tumor grafts derived from women with breast cancer authentically reflect tumor pathology, growth, metastasis and disease outcomes. Nat Med 2011;17:1514–20.
31. Fruman DA, Chiu H, Hopkins BD, Bagrodia S, Cantley LC, Abraham RT. The PI3K pathway in human disease. Cell 2017;170:605–35.
32. Wong KK, Engelman JA, Cantley LC. Targeting the PI3K signaling pathway in cancer. Curr Opin Genet Dev 2010;20:87–90.
33. Zardavas D, Phillips WA, Loi S. PIK3CA mutations in breast cancer: reconciling findings from preclinical and clinical data. Breast Cancer Res 2014;16:201.
34. Aertgeerts K, Skene R, Yano J, Sang BC, Zou H, Snell G, et al. Structural analysis of the mechanism of inhibition and allosteric activation of the kinase domain of HER2 protein. J Biol Chem 2011;286:18756–65.
35. Wang T, Xu Y, Sheng S, Yuan H, Ouyang T, Li J, et al. HER2 somatic mutations are associated with poor survival in HER2-negative breast cancers. Cancer Sci 2017;108:671–7.
36. Persky NS, Hernandez D, Do Carmo M, Brenan L, Cohen O, Kitajima S, et al. Defining the landscape of ATP-competitive inhibitor resistance residues in protein kinases. Nat Struct Mol Biol 2020;27:92–104.
37. Pimentel C, Becquet M, Lavoue V, Henno S, Leveque J, Ouldamer L. Ovarian metastases from breast cancer: a series of 28 cases. Anticancer Res 2016;36:4195–200.
38. Mathew A, Rajagopal PS, Villgran V, Sandhu GS, Jankowitz RC, Jacob M, et al. Distinct pattern of metastases in patients with invasive lobular carcinoma of the breast. Geburtshilfe Frauenheilkd 2017;77:660–6.
39. Jeselsohn R, Bergholz JS, Pun M, Cornwell M, Liu W, Nardone A, et al. Allele-specific chromatin recruitment and therapeutic vulnerabilities of ESR1 activating mutations. Cancer Cell 2018;33:173–86.
40. Toy W, Weir H, Razavi P, Lawson M, Goeppert AU, Mazzola AM, et al. Activating ESR1 mutations differentially affect the efficacy of ER antagonists. Cancer Discov 2017;7:277–87.
41. Robichaux JP, Elamin YY, Vijayan RSK, Nilsson MB, Hu L, He J, et al. Pan-cancer landscape and analysis of ERBB2 mutations identifies poziotinib as a clinically active inhibitor and enhancer of T-DM1 activity. Cancer Cell 2019;36:444–57.
42. Robichaux JP, Elamin YY, Tan Z, Carter BW, Zhang S, Liu S, et al. Mechanisms and clinical activity of an EGFR and HER2 exon 20-selective kinase inhibitor in non-small cell lung cancer. Nat Med 2018;24:638–46.
43. Kim JY, Lee E, Park K, Jung HH, Park WY, Lee KH, et al. Molecular alterations and poziotinib efficacy, a pan-HER inhibitor, in human epidermal growth factor receptor 2 (HER2)-positive breast cancers: combined exploratory biomarker analysis from a phase II clinical trial of poziotinib for refractory HER2-positive breast cancer patients. Int J Cancer 2019;145:1669–78.
44. Prelaj A, Bottiglieri A, Proto C, Lo Russo G, Signorelli D, Ferrara R, et al. Poziotinib for EGFR and HER2 exon 20 insertion mutation in advanced NSCLC: results from the expanded access program. Eur J Cancer 2021;149:235–48.
45. Sudhan DR, Guerrero-Zotano A, Won H, Ericsson PG, Servetto A, Huerta-Rosario M, et al. Hyperactivation of TORC1 drives resistance to the pan-HER tyrosine kinase inhibitor neratinib in HER2-mutant cancers. Cancer Cell 2020;37:258–9.
46. Zhao M, Scott S, Evans KW, Yuca E, Saridogan T, Zheng X, et al. Combining neratinib with CDK4/6, mTOR, and MEK inhibitors in models of HER2-positive cancer. Clin Cancer Res 2021;27:1681–94.